

## Electrochemical Study of Carbon Steel and 304 Stainless Steel Erosion Behavior in Sand-Containing Water

Teng Wu<sup>1,\*</sup>, Yixuan Liu<sup>1</sup>, Jie Qin<sup>1</sup>, Yan Wang<sup>2</sup>, Shengnan Ye, Xinguo Feng<sup>1</sup>, Shengli Chen<sup>3</sup>

<sup>1</sup> Jiangsu Key Laboratory of Coast Ocean Resources Development and Environment Security, Hohai University, Nanjing 210098, Jiangsu, China

<sup>2</sup> Hangzhou Jinghang Canal Second Channel Construction Investment Co., Ltd. Hangzhou 310000, Jiangsu, China

<sup>3</sup> CNOOC information technology Co., Ltd. Oceanographic information Center, Beijing 100013, China

\*E-mail: [wuteng@hhu.edu.cn](mailto:wuteng@hhu.edu.cn)

Received: 2 May 2020 / Accepted: 15 July 2020 / Published: 10 August 2020

---

The effects of rotational speed and sand concentrations on the wear behavior on carbon steel and stainless steel were investigated by open-circuit potential, polarization curves, electrochemical impedance spectroscopy and scanning electron microscopy. The mass loss rates of samples under each condition were determined. The erosion rates of both steels increased with the rotational speed and sand concentration, and the erosion rates of the 304 stainless steel were approximately one-tenth of the carbon steel for the same conditions in the sand-containing water. The erosion rate that was calculated from the polarization curve method was similar to the tested mass loss results, and can be used to determine the erosion rate in flowing sand-containing water.

---

**Keywords:** Erosion, stainless steel, carbon steel, electrochemical test

### 1. INTRODUCTION

Erosion is a key cause of metal-alloy degradation in many industrial fields [1]. When an alloy is exposed to a flowing slurry, its surface is eroded when the particle kinetic energy in the flowing slurry exceeds a threshold value [2, 3]. Erosion behavior tends to be ascribed to plastic deformation and material rupture on the surface. When the particles impinge on the alloys, the local current density immediately increases sharply. Previous studies suggest that alloys with a lower hardness experience more severe erosion, and the synergistic effect between erosion and corrosion may accelerate alloy degradation in aggressive environments [4, 5]. Therefore, it is important to study the erosion behavior, and the erosion–corrosion characteristics of alloys in their service environments.

Carbon steel is used widely in many fields because of its low cost, but its unsatisfactory corrosion resistance limits its application in certain environments [6, 7]. Higher corrosion-resistant alloys, such as stainless steel, have a protective passive film on the surface that results from the chromium content [8-11] and have attracted attention for use in these special environments [12, 13]. In this study, the effect of sand concentration and rotational speed on the erosion behavior of 304 stainless steel and carbon steel were investigated. The erosion rates of the stainless steel were approximately one-tenth of that of carbon steel under the same conditions in sand-containing water.

## 2. MATERIALS AND EXPERIMENTS

### 2.1 Materials

Medium carbon steel (CS) and stainless steel (SS) 200 mm × 10 mm × 3 mm plates were used. After being ground with emery paper up to No. 600, the steel samples were degreased by using alcohol and were washed with deionized water. The samples were dried by using cold air. The cleaned steel samples were coated with silica gel, with an area of 5.0 cm<sup>2</sup> retained in the middle for exposure to the sand-containing water. Standard medium sand, as shown in Figure 1 (a), was added to tap water at 20.0 g/L and 100 g/L. A scanning electron micrograph of the sand after 10 h of erosion testing at 750 rad is presented in Figure 1 (b).

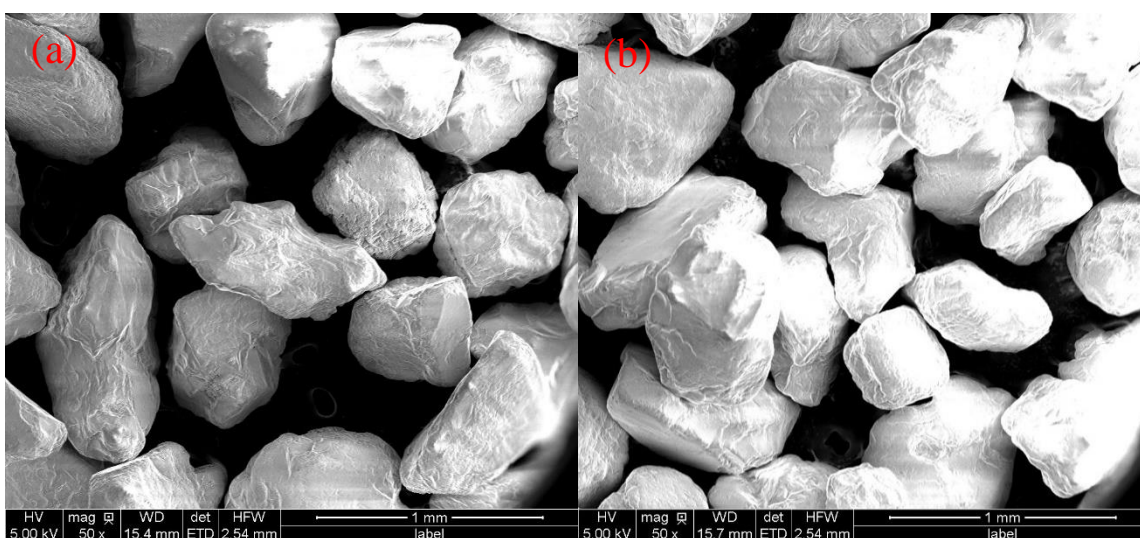


**Figure 1.** Micrographs of standard medium sand, (a) before erosion test, (b) after 10 h of erosion at 750 rad.

### 2.2 Experiments

Home-made equipment, as shown in Figure 2, was used to conduct the erosion tests. The prepared steel samples were fixed to the inside wall of the tank. Sand in the water was stirred by three impellers arranged 60° apart, as shown in Figure 2 (b). During the erosion tests, the flow velocity was

controlled by the motor rotational speed. To investigate the influence of flow velocity on the erosion rate of the two steels, 250 rpm, 500 rpm, and 750 rpm rotational speeds were used in the sand-containing water with concentrations of 20 g/L and 100 g/L.

After erosion for 9 h, results of the open-circuit potential, polarization curve, and electrochemical impedance spectroscopy (EIS) of the steel sample were obtained at 250 rpm, 500 rpm, and 750 rpm in the sand-containing water. The electrochemical tests were performed by using a CS 350 workstation (Corrtest instrument, China). The tested steel sample, a platinum plate, and a saturated calomel electrode were connected to the work electrode, counter electrode, and reference electrode. Every electrochemical test was repeated three times using a new sample. The steel sample mass losses were recorded, and mass loss rates were calculated. The steel surfaces after 10 h of erosion were examined by using a Hitachi S-4700 scanning electron microscope.

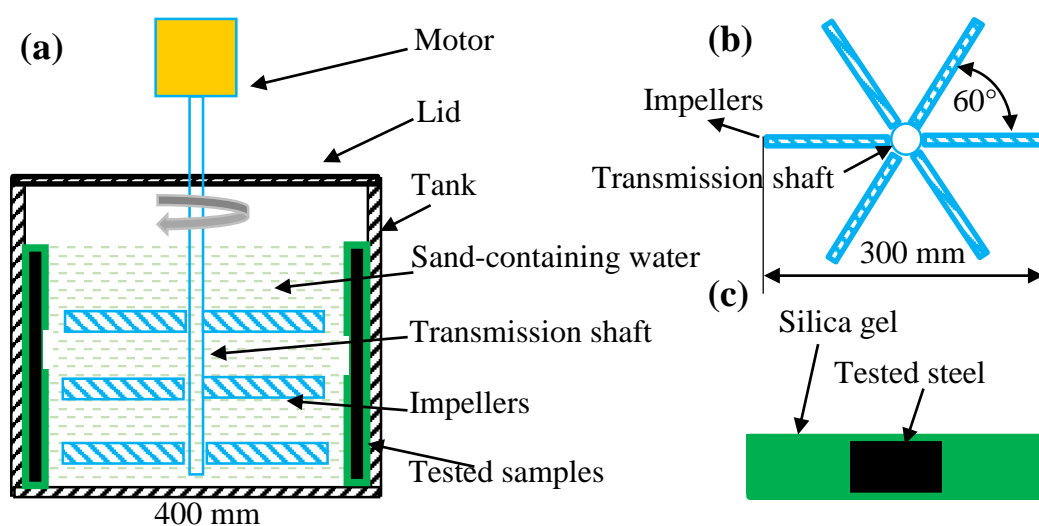


**Figure 2.** Schematic representation of erosion test apparatus: (a) front view of test apparatus, (b) top view of agitator, (c) schematic of sample processing.

### 3. RESULTS AND DISCUSSION

#### 3.1 Open-circuit potential

The open-circuit potentials of the wearing steels at different rotational speeds were determined as shown in Table 1. The open-circuit potentials of the two steels decreased with rotational speed, and those of the stainless steels were influenced more by the rotational speed. The stainless-steel potential was higher than that of the carbon steel. When the sand concentration changed from 20 g/L to 100 g/L, the open-circuit potentials of the carbon and stainless steel shifted slightly negatively, which suggests that the erosion of the two steels intensified with an increasing rotational speed and sand concentration. The 304 stainless steel showed a higher erosion resistance than that of the carbon steel counterpart.

**Table 1.** Calculated open-circuit potential and corrosion current density from polarization curves for steel erosion at different rotational speeds in sand-containing water.

Rotational speeds/rpm	Open-circuit potential / $V_{\text{saturated calomel electrode}}$				Corrosion current density ( $i_{\text{corr-pc}}$ ) / $\mu\text{A}\cdot\text{cm}^{-2}$			
	CS-20g/L	CS-100g/L	SS-20g/L	SS-100g/L	CS-20g/L	CS-100g/L	SS-20g/L	SS-100g/L
250	-0.272	-0.307	-0.133	-0.173	4.3616	6.0328	0.58289	0.70194
500	-0.277	-0.311	-0.201	-0.218	5.0226	6.1793	0.94201	1.0009
750	-0.284	-0.313	-0.236	-0.255	5.9252	6.3075	1.0318	1.4639

### 3.2 Polarization curves

Polarization curves of the two steels were obtained when the steel samples were eroded at different rotational speeds in the sand-containing water. Figure 3 shows no visible change in the cathodic polarization curves when the rotational speed and sand concentration increased. The anodic polarization curves of the two steels increased with the rotational speed and sand content, especially for the stainless-steel samples. The cathodic reaction, as shown in equation (1), is not affected by rotational speed and sand concentration, because the dissolved oxygen concentration in water was saturated under the experimental conditions used (open to air). An insignificant change was observed in the cathodic curves.



When the steel surface was impacted by the high-speed particles (sand) in water, the internal energy of the steel substrate was enhanced, which increased the activity and accelerated the anodic dissolution of the steel samples [14, 15]. As shown in Figure 3, the anodic current densities of the two steels increased with rotational speed and sand content. The corrosion current densities ( $i_{\text{corr-pc}}$ ) of the eroding steels were calculated from the polarization curves as shown in Table 1. The corrosion current densities of the two steels increased with the rotational speed and sand content. When the sand content increased from 20 g/L to 100g/L, the corrosion current densities of the stainless steel and the carbon steel increased by an average of 22.6% and 22.8%, respectively. However, the corrosion current densities of the steels increased by 92.8% and 20.0%, respectively, as the rotational speed increased from 250 to 750 rpm. The corrosion current densities of the carbon steel were much higher than those of the stainless steel, and the current density of the carbon steel was ~4–9 times (average of ~6.3 times) that of the stainless steel counterpart under the same conditions. The polarization curve results, together with the open-circuit results in Table 1, confirm that the stainless steel presented a higher erosion resistance than that of the carbon steel, and the erosion rates of the two steels with an increasing rotational speed and sand content.

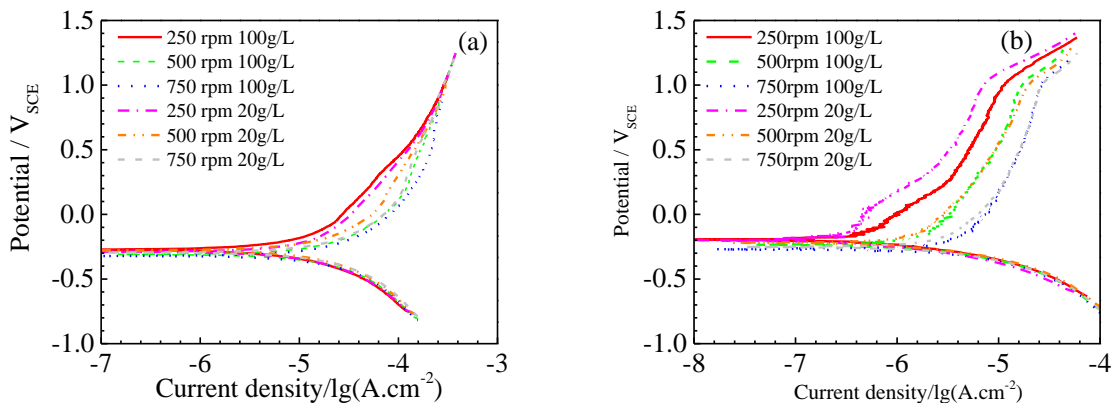


**Figure 3.** Polarization curves of eroding steels at different rotational speeds in the sand-containing water, (a) carbon steel, (b) stainless steel.

### 3.3 Electrochemical impedance spectroscopy

The electrochemical impedance spectroscopy of the eroding carbon steel and stainless steel in the sand-containing water were tested, and the results are shown in Figures 4 and 5, respectively. Two capacitive loops are visible in the Nyquist plots of the carbon and stainless steels, which is consistent with earlier studies [16]. The stainless-steel impedances were higher than those of the carbon steel samples. The arc radius at a low frequency was lower than that at a high frequency for the eroding carbon steel, whereas the reverse scenario was observed for stainless steel under the same conditions.

Previous studies [17, 18] have proposed that an equivalent circuit in Figure 6 fits the experimental EIS impedance data, where  $R_s$  is the solution resistance,  $R_f$  and  $C_f$  are the resistance and capacitance of the films on the steel surface, and  $R_{ct}$  and  $C_{ct}$  represent the polarization resistance of the corrosion process and the double-layer capacitance [17,19]. The fitting results of the film resistance ( $R_f$ ) and polarization resistance ( $R_{ct}$ ) are presented in Table 2. The film resistance ( $R_f$ ) of the two steels is lower than its polarization resistance ( $R_{ct}$ ), which agrees with an earlier study by Sahoo [20].

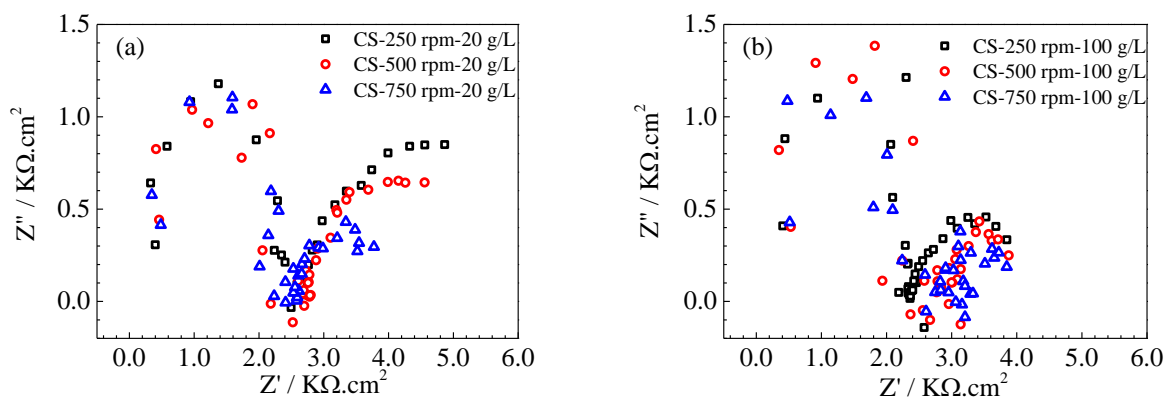


**Figure 4.** Nyquist plots for eroding carbon steel at different rotational speeds, (a) in 20 g/L sand, (b) in 100 g/L sand.

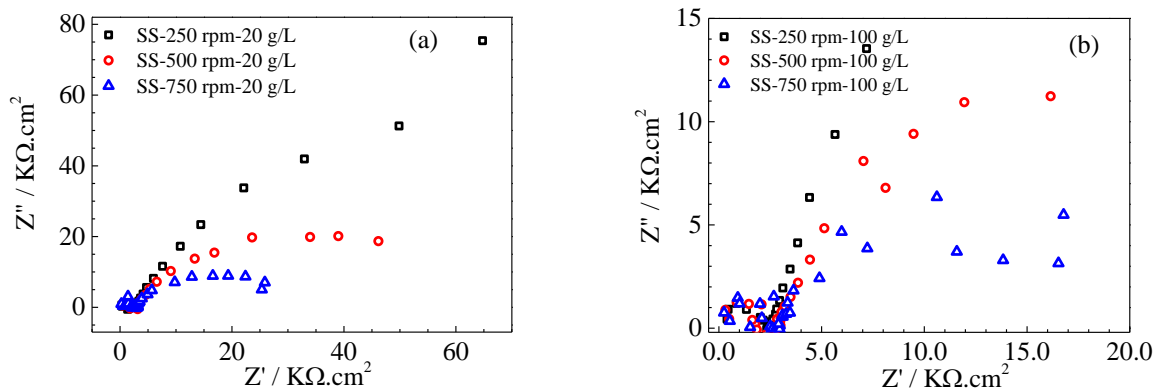


**Figure 5.** Nyquist plots for eroding stainless steel at different rotational speeds, (a) in 20 g/L sand, (b) in 100 g/L sand.

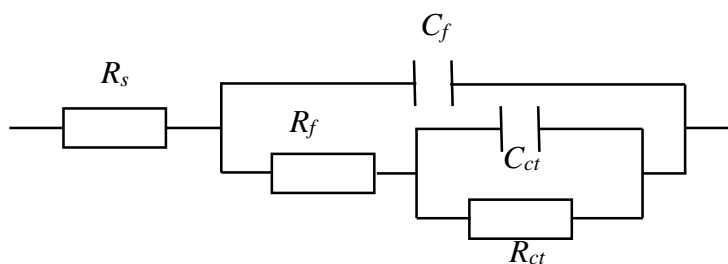


**Figure 6.** Equivalent electrical circuit for modeling impedance spectra data.

**Table 2.** Fitting film resistance ( $R_f$ ) and polarization resistance ( $R_{ct}$ ) of eroding steel samples in sand-containing water at different rotational speeds.

Rotational speeds/rpm	$R_f / \Omega.cm^{-2}$				$R_{ct} / \Omega.cm^{-2}$			
	CS-20g/L	CS-100g/L	SS-20g/L	SS-100g/L	CS-20g/L	CS-100g/L	SS-20g/L	SS-100g/L
250	2338	2200	2606	2377	1781	1095	81230	121900
500	2394	2496	2640	2941	1499	867.5	38510	27130
750	2175	2534	2688	2633	977.6	754.1	20740	12520

**Table 3** Corrosion current densities ( $i_{corr-EIS}$ ) of eroding steels calculated from polarization resistance ( $R_{ct}$ ) in EIS results at different rotational speeds in sand-containing water.

Rotational speeds/rpm	Corrosion current density ( $i_{corr-EIS}$ ) / $\mu A.cm^{-2}$			
	CS-20g/L	CS-100g/L	SS-20g/L	SS-100g/L
250	14.599	23.744	0.32008	0.21329
500	17.345	29.971	0.67515	0.95835
750	26.596	34.478	1.2536	2.0767

The film resistances ( $R_f$ ) of the stainless-steel samples were slightly higher than those of the carbon steel ones, which suggests a higher passivity of the former steel. The film resistances of the two eroded steels were not influenced significantly by the rotational speeds, which indicates that the films of the two steels were eroded by the addition of sand in the water. The polarization resistance ( $R_{ct}$ ) of the steels decreases with rotational speed and sand content in the water. The  $R_{ct}$  of the stainless-steel samples was almost two orders of magnitude higher than that of the carbon steel. The fitted EIS results indicate that the stainless steel exhibits a higher erosion resistance than the carbon steel, and films on the carbon and 304 stainless steels were eroded by sand addition.

The corrosion current densities ( $i_{corr-EIS}$ ) of the eroding steels were calculated from the fitted polarization resistance ( $R_{ct}$ ) [21, 22]:

$$i_{corr-EIS} = B / R_{ct} \quad (2)$$

$B$  is the Stern–Geary constant from sand erosion on the steel, the surface is assumed to be active, and 26 mV/dec was chosen for  $B$ . As shown in Table 3, the  $i_{corr-EIS}$  for the carbon steel was ~4.25 times that of the same ones from the polarization curves (Figure 4). However, the corrosion current density from the EIS ( $i_{corr-EIS}$ ) was similar to that calculated from the polarization curves for the stainless steel. The  $i_{corr-EIS}$  of the two steels increased with rotational speed and sand content.

### 3.4 Mass loss rates

The mass losses ( $\Delta m$ ) of the carbon steel and 304 stainless steel were recorded after 10 h of erosion in the sand-containing water at different rotational speeds, and the mass loss rates ( $v_m$ ) are presented in Figure 7 (a). To compare the corrosion current densities that were calculated from the polarization curves and fitting polarization resistance ( $R_{ct}$ ) in the EIS, the mass loss rates were transformed to the corrosion current densities ( $i_{corr-wl}$ , A.cm<sup>-2</sup>) [23, 24]:

$$i_{corr-wl} = (A \times n \times F \times v_m) / M \quad (3)$$

where  $A$  is the exposed sample area,  $n$  is the electron valence of the metal,  $F$  is the Faraday's constant (1 F = 26.8 A.h),  $v_m$  is the tested mass loss rate (g.cm<sup>-2</sup>.s<sup>-1</sup>), and  $M$  is the material molar mass. In this study, the  $M/n$  ratios for the 304 stainless steel and carbon steel were 18.99 and 18.62, respectively, according to the ASTM G102 standard [25]. The corresponding corrosion current densities of the two steels from the mass losses are shown in Figure 7(b). The mass loss rates ( $v_m$ ) and the corresponding corrosion current densities ( $i_{corr-wl}$ ) of the carbon steel are higher than those of the stainless-steel counterpart under the same conditions.  $v_m$  and  $i_{corr-wl}$  increased with rotational speed and sand content in the water, which is consistent with the electrochemical tests results in Tables 1 and 3.

To investigate the effectiveness of the corrosion current density from the EIS data and polarization curves on the eroding samples, the aforementioned corrosion current densities were compared with those from the mass loss results, and the results are shown in Figure 8. For the eroding carbon steel, as shown in Figure 8 (a), the corrosion current densities from the polarization curves is closer to the mass loss results, whereas those from the EIS data were 3–5 times to the mass loss results. Therefore, the polarization curve may be an effective method to determine the corrosion current densities of the eroding carbon steel in the sand-containing solution. However, for the eroding stainless steel, as

shown in Figure 8 (b), the corrosion current densities from the polarization curves and EIS data are similar to the mass loss results, which indicates that the two electrochemical tests are suitable for assessing the erosion rate of the stainless steel.

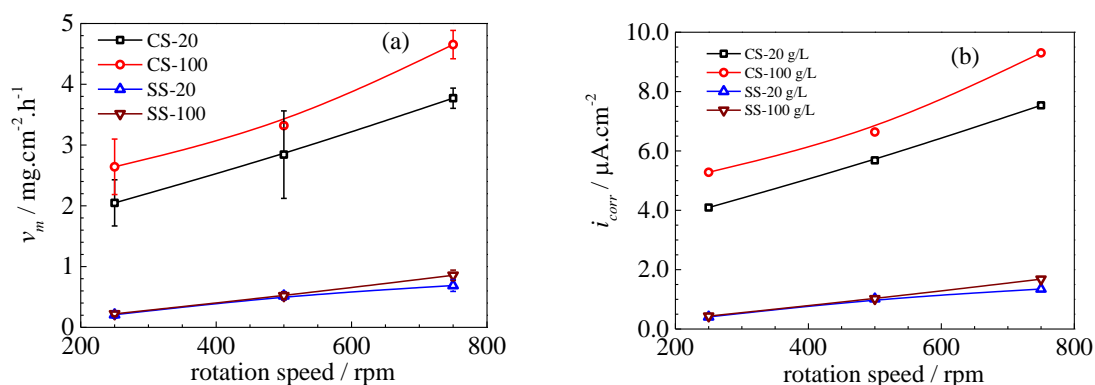


**Figure 7.** Mass loss rates ( $v_m$ ) and corresponding corrosion current densities ( $i_{corr-wl}$ ) of eroding steels from mass losses at different rotational speeds in sand-containing water.

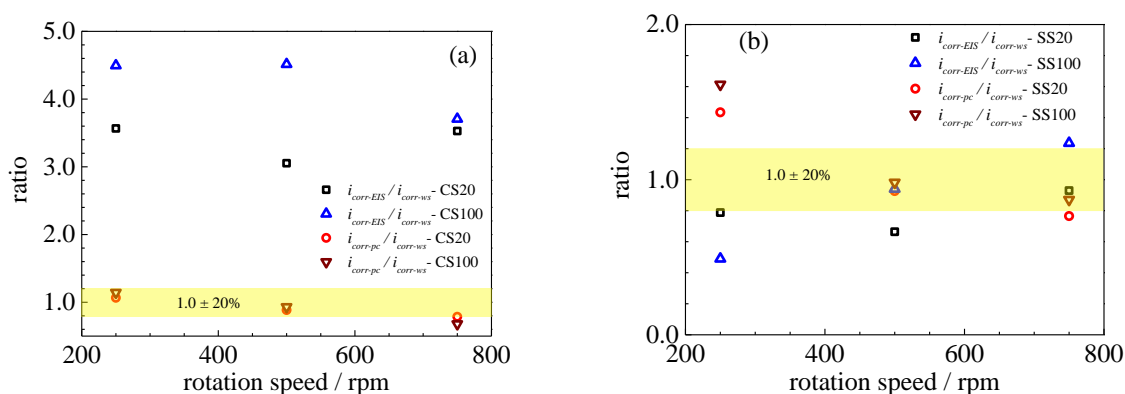


**Figure 8.** Ratios of corrosion current densities from EIS data and polarization curves to mass loss results, (a) carbon steel, (b) stainless steel.

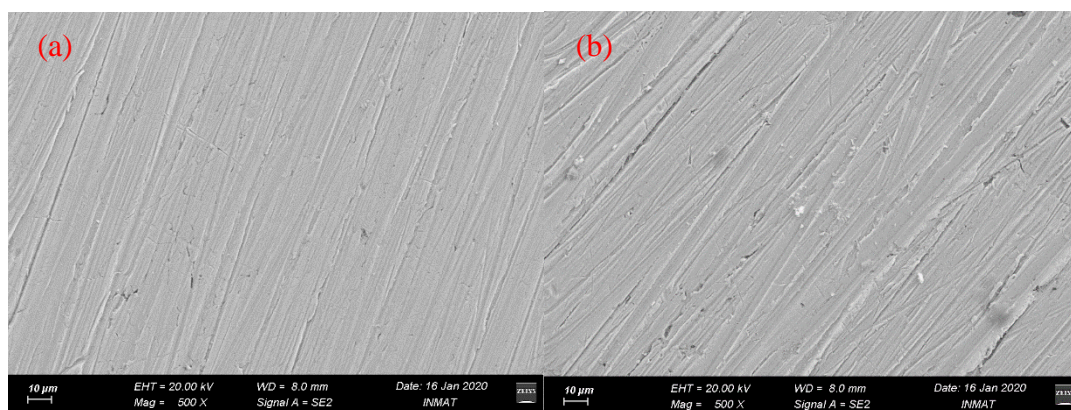
### 3.5 Surface morphology

After being eroded for 10 h in the sand-containing solution at different rotational speeds, the eroded surfaces of the two steels were studied, and the results are shown in Figures 9 and 10.

The carbon steel surface roughness decreased with rotational speed (Figure 9), whereas that of the stainless-steel surface was not influenced significantly by the rotational speed (Figure 10). As the mass loss rate results shows (Figure 7), the erosion rates of both steels increased with the rotational speed, but those of the carbon steel were almost one order of magnitude higher than those of the stainless steel. As shown in Figure 9, scratches caused by grinding decreased gradually on the carbon steel surface when the rotational speed increased. However, at a lower erosion rate, the scratches on the stainless-steel surface did not show any visible change with increasing rotational speed, after being eroded for 10 h. The surface results confirmed that the 304 stainless steel had a higher erosion resistance than that of the carbon steel, and the erosion rate of the two steels increased with rotational speed.



**Figure 9.** Morphology of eroded surface of carbon steels at different rotational speeds in sand-containing solution. (a) 250 rpm, (b) 500 rpm, (c) 750 rpm.



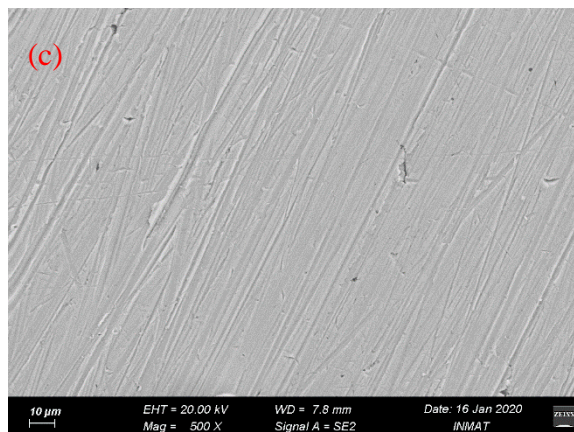


**Figure 10.** Morphology of eroded surface of stainless steels at different rotational speeds in sand-containing solution. (a) 250 rpm, (b) 500 rpm, (c) 750 rpm.

#### 4. CONCLUSIONS

1. The erosion rates and mass loss rates of the carbon steel and 304 stainless steel increased with an increase in rotational speed and sand concentration.
2. The 304 stainless steel showed a higher erosion resistance than that of the carbon steel, and the erosion rate of the stainless steel was approximately one-tenth of the carbon steel in the sand-containing water.
3. Compared with the mass loss results, the erosion rate from the EIS and polarization curve methods were acceptable for the stainless steel, whereas that from the polarization curve method was more suitable for carbon steel in the flowing sand-containing water.

#### ACKNOWLEDGEMENTS

The Science and Technology Foundation of Zhejiang Provincial Department of Transport (2020015), China Railway Construction Investment Group Co., Ltd. 2020 Science and Technology Research and Development Plan (2020-B07), and the Fundamental Research Funds for the Central Universities (2019B12114) are gratefully acknowledged.

#### References

1. M. Jones, R. J. Llewellyn, *Wear*, 267 (2009) 2003.
2. B. T. Lu, J. L. Luo, *J. Phys. Chem. B*, 110 (2006) 4217.
3. F. Mohammadi, J. Luo, *Corros. Sci.*, 52 (2010) 2994.
4. B. Vyas, I. L. H. Hansson, *Corros. Sci.*, 30 (1990) 761.
5. C. T. Kwok, F. T. Cheng, H. C. Man, *Mater. Sci. Eng., A*, 290 (2000) 145.
6. R. Réquíz, S. Camero, A. L. Rivas, *Microsc. Microanal.*, 11 (2005) 1992.
7. M. A. Maes, M. Dann, M. M. Salama, *Reliab. Eng. Syst. Safe.*, 93 (2008) 447.
8. J.H. Baek, Y.P. Kim, W.S. Kim, Y.T. Kho, *Int. J. Pres. Ves. Pip.*, 78 (2001) 351.
9. D. D. Macdonald, *J. Electrochem. Soc.*, 139 (1992) 3434.

10. C. Y. Chao, *J. Electrochem. Soc.*, 128 (1981) 1187.
11. J. Li, Y. G. Zheng, J. Q. Wang, Z. M. Yao, Z. F. Wang, W. Ke, *Wear*, s186-187 (1995) 562.
12. I. Finnie, *J. Mater. Sci.*, 2 (1967) 682.
13. R.J.K. Wood, *Wear*, 261 (2006) 1012.
14. R.W. Hertzberg, R.P. Vinci, J.L. Hertzberg, *Deformation and Fracture Mechanics of Engineering Materials*, (1996), Wiley, New York.
15. T. Xu, L. Zheng, K. Wang, R. Misra, *Int. Mater. Rev.*, 58 (2013) 263.
16. A.S. Hamdy, A.G. SaEh, M.A. Shoeib, Y. Barakat, *Electrochim. ACTA.*, 52 (2007) 7068.
17. X. Feng, X. Zhang, Y. Xu, R. Shi, X. Lu, L. Zhang, J. Zhang, D. Chen, *Eng. Fail. Anal.*, 98 (2019) 49.
18. X. Feng, X. Lu, Y. Zuo, N. Zhuang, D. Chen, *Corros. Sci.*, 103 (2016) 223.
19. X. Feng, Y. Tang, Y. Zuo, *Corros. Sci.*, 53 (2011) 1304.
20. G. Sahoo, R. Balasubramaniam, *Corros. Sci.*, 50 (2008) 131.
21. X. Feng, X. Lu, Y. Zuo, N. Zhuang, D. Chen, *Corros. Sci.*, 103 (2016) 66.
22. X. Feng, Y. Tang, X. Zhao, Y. Zuo, J. Wuhan. Univ. Technol.-Mater. Sci. Ed., 27 (2012) 994.
23. N. Khayatan, H.M. Ghasemi, M. Abedini, *Wear.*, 15 (2017) 154.
24. E. McCafferty, Mechanically assisted corrosion. In *Introduction to Corrosion Science*, (2010), Springer, New York.
25. ASTM Standard G 102-04, *ASTM International*, USA, 2004.